Curr Cardiovasc Imaging Rep (2014) 7:9279
DOI 10.1007/s12410-014-9279-8

High Risk Plaque Features on Coronary CT Angiography

Andrea Bartykowszki · Csilla Celeng · Mihály Károlyi · Pál Maurovich-Horvat

Published online: 17 June 2014

Abstract Coronary computed tomography angiography (CCTA) is a non-invasive imaging technique that can detect, characterize and quantify coronary atherosclerotic plaques in routine clinical settings. The distinct morphological features of vulnerable plaques and stable lesions provide an opportunity for CCTA to identify high-risk plaque features and guide stratified therapeutic interventions. Morphological plaque characteristics, such as large plaque volume, positive remodelling, low CT attenuation, spotty calcification and the napkin-ring sign have been linked to elevated risk of acute coronary syndrome. Recent advances in computational fluid dynamics enabled functional plaque assessment through endothelial shear stress and lesion specific fractional flow reserve calculation. The comprehensive, morphological and functional plaque assessment may improve the identification of vulnerable coronary lesions.

Keywords Coronary CT angiography · Coronary atherosclerosis · Vulnerable plaque · High plaque features

Introduction

Cardiovascular diseases are the leading cause of morbidity and mortality in most countries around the world. Despite significant progress in the prevention and treatment strategies, an estimated 1.1 million Americans will suffer a major adverse coronary event in 2014 and 34 % of those will die of it. The most common cause of coronary heart disease is the atherosclerosis of the coronary arteries [1]. Coronary atherosclerosis is a chronic, multifocal disease in which the complex interactions of pathological processes precipitate the accumulation of atherosclerotic plaques [2–4]. According to autopsy studies the majority of cardiac events are caused by plaque rupture and subsequent thrombosis [5–7]. The morphology and structure of rupture-prone plaques is different from stable lesions, which provide potential target for non-invasive imaging techniques to identify high-risk plaques before they cause clinical event [8]. The cardiovascular event rate is strongly associated to the presence and extent of atherosclerosis therefore the characterization and quantification of coronary artery disease is of utmost importance in order to identify the patients at highest risk to suffer an acute coronary event.

Coronary CT angiography (CCTA) and its ability to detect and quantify coronary artery disease (CAD) have evolved rapidly during the past decade. Large clinical studies and mate-analyses have proved that CCTA has an unparalleled diagnostic performance to identify obstructive CAD, with a sensitivity of 85–100 %, and specificity of 85–99 % [9–11]. To date CCTA is the only non-invasive diagnostic imaging modality that allows the assessment of luminal narrowing and provides direct information regarding the atherosclerotic plaques. The excellent image quality of state-of-the-art CT scanners enables robust plaque quantification and characterization, which opens new avenues in cardiovascular risk stratification and anti-atherosclerotic therapy response monitoring. The goal of CCTA plaque characterization is to identify the vulnerable plaque and ultimately the vulnerable patient. Therefore, at the dawn of personalized medicine CCTA might have an important role to guide stratified therapeutic approaches based on coronary plaque characteristics. In this review article we provide detailed description of the current status of CCTA on morphologic and functional plaque characterization, in order to identify vulnerable patients, who are at highest risk to develop acute coronary syndromes.

This article is part of the Topical Collection on *Cardiac Computed Tomography*

A. Bartykowszki · C. Celeng · M. Károlyi · P. Maurovich-Horvat (✉)
MTA-SE Lendület Cardiovascular Imaging Research Group, Heart and Vascular Center, Semmelweis University, 68 Varosmajor ut, 1122 Budapest, Hungary
e-mail: p.maurovich.horvat@mail.harvard.edu

The Concept and Morphologic Features of Vulnerable Plaque

Histopathologic investigations have demonstrated that most of the acute coronary events are caused by the sudden thrombotic occlusion of the coronary lumen due to atherosclerotic plaque rupture [12]. These atherosclerotic lesions are characterized by large necrotic core, which is covered by a ruptured thin layer of fibrous cap. Precursor lesions of plaque rupture are termed as thin cap fibroatheroma (TCFA) in histology, with a cap thickness of <65 μm. Importantly, the current CT technology cannot depict and measure fibrous cap thickness due to the limited spatial resolution of the scanners (≈400 μm). However, high-risk plaques tend to be large, with a necrotic core length of 2 to 17 mm (mean 8 mm). In addition the area of lipid rich, necrotic core is larger than 1 mm^2 in 80 % of cases [13]. In an *ex vivo* study CCTA safely identified lesions with at least 1 mm thickness [14]. Thus, it is reasonable to assume that in some extent CCTA is able to visualize and quantify coronary plaque features that are characteristic of vulnerable lesions. The concept of rupture prone vulnerable plaque underwent remarkable evolution during the past decade. From a sole morphometric plaque feature it became a probabilistic concept that refers to plaques that may be associated with future coronary events. CCTA can detect certain compositional and geometrical features of plaques that have been associated with cardiac events. In the following sections we provide an overview regarding the potential targets of CCTA imaging to identify vulnerable plaques with an increased risk to rupture and cause acute coronary event.

Plaque Burden

Intravascular ultrasound (IVUS) is the clinical reference standard for the quantitative evaluation of coronary atherosclerosis. According to the results of the IVUS based Providing Regional Observations to Study Predictors of Events in the Coronary Tree (PROSPECT) trial increased plaque burden is the strongest predictor of recurrent coronary events in patients who suffered acute coronary syndrome (ACS) [15]. Importantly, the use of IVUS is limited in patients with severe coronary stenosis or occlusion. In addition, IVUS-based plaque measurements are typically limited to 1 or 2 coronary segments, which might limit its applicability to assess the overall plaque growth [16]. The state-of-the-art CT scanners with a sub-millimeter spatial resolution provide a unique opportunity to detect, quantify and characterize coronary plaques globally, along the entire coronary tree (Figs. 1 and 2).

The diagnostic performance of CCTA to detect coronary atherosclerotic plaques compared to IVUS has improved over the past decade. Pioneer studies using 16-slice scanners demonstrated an overall moderate diagnostic accuracy. The sensitivity to detect non-calcified plaque (NCP) was 53-81 % and the specificity 80-87 % as compared to IVUS. On the other hand, studies using 64-slice scanners yielded sensitivity values of 83-97 % with specificity around 89 % [17–20]. Despite the improved sensitivity values, the specificity has not changed significantly with the newer scanner technologies, probably because of the minor improvements in the in-plane resolution and contrast resolution. According to a recent meta-analysis the combined sensitivity and specificity of CCTA to detect coronary plaque is 90 % (95 % CI: 83 % to 94 %) and 92 % (95 % CI: 90 % to 93 %), respectively [21••].

During recent years several studies investigated the accuracy of CCTA against IVUS regarding the assessment of plaque burden. The accuracy was influenced by the plaque composition. The non-calcified and mixed plaque volumes were underestimated, whereas the volume of calcified plaque was overestimated [22, 23]. Brodoefel et al. used a semiautomated plaque quantification tool and demonstrated a good correlation between CCTA and IVUS regarding the volume of non-calcified plaque, however CT overestimated the total plaque volume and the volume of calcification [18]. Recently, the accuracy of automated quantification of coronary plaque by CCTA performed with modern CT scanners was successfully validated against grey scale IVUS and virtual histology IVUS [21••, 24••, 25]. Moreover, the reproducibility of such automated 3-dimensional quantification software for plaque burden was excellent with an intra-class correlation value of 0.88 (95 % CI 0.74 – 0.95) [24••]. Notably, the automated coronary plaque assessment tools demonstrated a good intraplatform reproducibility, however the interplatform variability proved to be significant [26]. Therefore, it is advisable to use the same software tool in longitudinal plaque quantification studies until industry standards are developed to guarantee reproducible plaque assessment regardless of the type of scanner and software used.

Plaque assessment with CCTA in patients with stable angina pectoris and patients who suffered acute coronary syndromes demonstrated significant differences in plaque burden between these two patient populations. Recent cross-sectional clinical investigations found that the culprit lesions in patients with unstable angina or ACS have a larger volume than stable plaques in SAP patients (193-313 mm^3 vs. 104-118 mm^3, $p<0.001$) [27, 28] These findings are in line with previous histological observations that described larger dimensions for culprit lesions compared to stable fibrotic plaques [13]. Moreover, several CCTA studies have demonstrated a strong prognostic value of increased plaque volumes. Motoyama et al. showed that SAP patients who suffered ACS during a follow-up period of 27±10 months had larger coronary plaque volume at baseline (134.9±14.1 mm^3 vs. 57.8±5.7 mm^3, $p<0.001$) [29]. In a subsequent prospective study Kristensen et al. described that total volume of non-obstructive non-calcified plaque is independently associated with recurrent

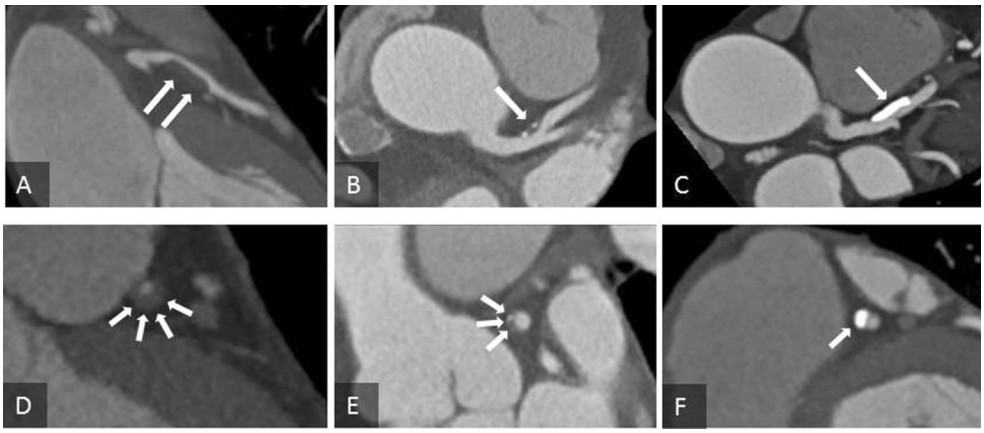

Fig. 1 Double oblique reformations of CCTA images represent longitudinal sections of proximal LAD segments (upper image panels) and cross-sections of the same segments (lower panels). Panels **a** and **d**: non-calcified plaque with positive remodelling; Panels **b** and **e**: partially calcified plaque with spotty calcification; Panels **c** and **f**: calcified plaque. *CCTA* coronary computed tomography angiography. *LAD* left anterior descending coronary artery

acute coronary event in patients who suffered non-ST-segment elevation myocardial infarction (NSTEMI). During the 16 months follow-up period NCP was independently associated with the recurrent acute events with a hazard ratio of 1.18 per 100 mm^3 non-calcified plaque volume increase. Notably, the amount of calcified lesions was not associated with an increased risk. [30••] Similarly, Versteylen et al. found that plaque burden as assessed by a semiautomated software tool provided incremental prognostic value over traditional risk factors and conventional CT readings. Patients who suffered ACS had a larger total NCP volume at baseline compared to patients who did not develop ACS (28 mm^3 vs. 4 mm^3, $p<0.001$) [31].

Plaques with Low CT Attenuation

Plaques prone to rupture contain large, lipid-rich necrotic core, whereas stable lesions are characterized by the fibrous plaque components [32]. Therefore, the differentiation of lipid-rich

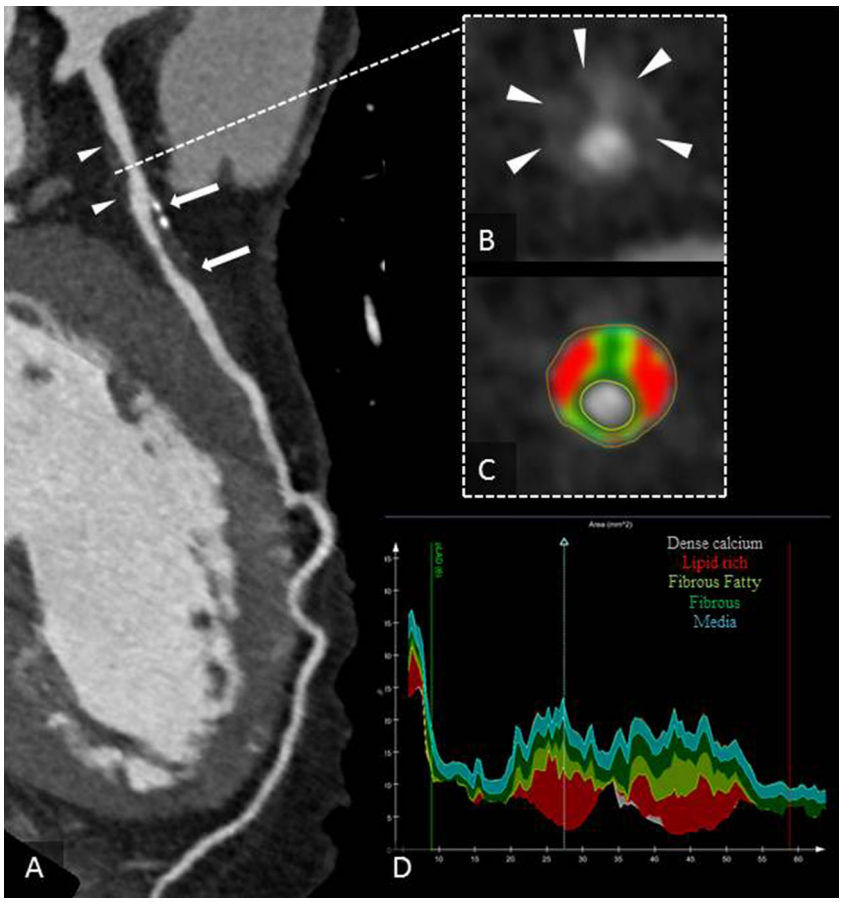

Fig. 2 Representation of plaque quantification using dedicated semiautomated software tool in CCTA data set. Panel **a**: LAD curved multiplanar reformation, *white arrowheads* show a non-calcified plaque with high risk features (positive remodelling and low mean plaque attenuation); *white arrows* indicate a partially calcified plaque with high risk features (positive remodelling, low mean plaque attenuation and spotty calcification). Panel **b** and **c**: plaque cross-section at the site indicated with *dashed line*. The plaque cross-section shows a large non-calcified plaque (*arrow heads*). The colour overlay in panel **c** indicates areas of low CT attenuation (*red colour*). Panel **d**: The graph illustrates the areas of different plaque components, x axis: distance fromthe LM orifice; y axis: area in mm^2. *CCTA* coronary computed tomography angiography, *LAD* left anterior descending coronary artery, *LM* left main stem, *Ca* calcium

versus fibrous plaques is desirable, as it might provide valuable information regarding plaque vulnerability (Fig. 2). A study conducted by Kopp et al. was the first to demonstrate the feasibility of plaque attenuation measurements and limited plaque differentiation based on intra-plaque CT numbers [33]. They have demonstrated that plaques described as "soft" by intravascular ultrasound (IVUS) had lower CT numbers as compared to "intermediate" and "calcified" lesions [33]. Subsequent studies differentiated three types of plaques depending on the presence and amount of calcification: calcified, non-calcified and partially calcified (mixed) plaques (Fig. 1). A significant difference in Hounsfield units (HU) was observed between calcified and non-calcified plaque components (mean values across studies, 490 HU and 75 HU, respectively) [20, 23, 34–38]. In an *ex vivo* IVUS and CCTA study Becker et al. showed that the mean CT attenuation of lipid-rich lesions was 47±9 HU and predominantly fibrotic plaques showed a 104±28 HU mean attenuation [35]. Marwan et al. have used histogram analysis of the intraplaque pixel HU distribution and found significantly lower mean CT numbers of lipid-rich plaques (67±31 HU) compared to fibrotic plaques (96±40 HU) [39]. The pixel based plaque CT number analysis was recently validated by an *ex vivo* study which demonstrated that intraplaque area of >25 % of pixels with <60 HU had a good accuracy to detect lipid rich atherosclerotic lesions (sensitivity = 73 %, specificity = 71 %) [40]. Vulnerable plaques with thin fibrotic cap and large necrotic core showed lower CT numbers compared to stable, fibrotic lesions in two recently published clinical studies comparing CCTA assessment with optical coherence tomography (OCT, 35-45 HU vs. 62-79 HU, $p<0.001$) [41–43].

Nevertheless, despite the significant difference in the average CT numbers, there is wide variability and substantial overlap between the CT numbers of these two plaque components [22, 23, 36, 44]. This can be explained by the similar chemical composition of lipid-rich and fibrous plaques, furthermore by the limited spatial and contrast resolutions of CT scanners. In addition, the intraluminal contrast enhancement, the tube voltage and the reconstruction filter also influence the CT numbers of coronary plaques [38, 45–47]. Therefore, the differentiation between lipid-rich and fibrous plaques based on CT numbers remains to be challenging [48]. Despite the limitations associated with plaque HU assessment, longitudinal studies have consistently demonstrated that plaques with low CT attenuation have an increased risk to cause acute coronary events. Motoyoma et al. has demonstrated that plaques with <30HU mean attenuation are more frequent in patients who suffered ACS compared to patients with SAP (79 % versus 9 %, $p<0.0001$) [49]. Subsequent clinical investigations have confirmed these findings, and reported that the mean plaque attenuation was lower in patients with ACS versus patients with SAP (40-86 HU vs, 97-144 HU, $p<0.01$) [27, 50, 51].

Positive Remodelling

The compensatory expansion of the vessel wall with the enlargement of the atherosclerotic lesion called positive remodelling, and results a delayed onset of luminal narrowing. This phenomenon was described by Glagov et al. in 1987 [52]. Histopathologic investigations have demonstrated that ruptured coronary plaques of patients who died suddenly tend to be large and occupy more than half of the vascular cross-sectional area [53]. However, due to positive remodelling these lesions do not cause significant narrowing in approximately two-thirds of the cases [54••]. Remodelling index (RI) is the ratio of the vessel area at maximal luminal narrowing and the reference vessel area (average of the proximal and distal reference areas), (Fig. 1, panel a) [55, 56]. The cut-off value for positive remodelling was defined by IVUS studies as ≥1.05 or >1.0, however, due to the limited spatial resolution of CCTA, Gauss et al. suggested to use a threshold of ≥1.1 to define positive remodelling in CT [39, 56]. The CCTA assessment of remodelling index was validated in clinical studies using IVUS as a reference standard [24••, 39, 55]. Coronary plaques with positive remodelling on CCTA were demonstrated to have larger amount of necrotic core and a higher prevalence of TCFA as assessed by VH-IVUS [57]. Moreover, CCTA derived remodelling index was higher in vulnerable lesions defined as TCFA as compared to stable lesions in two recently published clinical investigations where OCT was used as the reference standard (1.14 vs. 0.95 and 1.14 vs. 1.02, both $p<0.0001$) [41, 42]. In addition, the authors suggested a remodelling index threshold of 1.08, which had the best diagnostic performance to identify TCFA [45]. In a study by Motoyama et al. positive remodelling was strongly associated with culprit plaques in patients with ACS (ACS 87 %, SAP 12 %, $p<0.0001$). A landmark study –conducted by the same investigators– has enrolled 1059 patients and demonstrated that plaques with positive remodelling and/or with low plaque attenuation were independent predictors of ACS during the 27±10 months follow-up period (hazard ratio: 22.8, 95 % confidence interval: 6.9 to 75.2, $p<0.001$) [29]. To put these results in a perspective, one in five patients with at least on of these high-risk CT plaque features (positive remodelling, low CT attenuation plaque) will have an event in 1-3 years, which is very similar to the patients with high risk plaques as defined by VH-IVUS in the PROSPECT trial [15, 29].

Spotty Calcium

The presence of calcification indicates advanced coronary atherosclerosis [58]. A strong correlation was observed between coronary calcification and coronary atherosclerotic plaque burden, furthermore, high calcium score is a strong independent cardiovascular risk factor [59–61]. However, the

local effect of calcification on plaque stability is controversial [62–64]. In IVUS studies spotty calcium was associated with accelerated disease progression in patients with SAP and it was related to culprit plaques in ACS patients [65, 66]. The definition of spotty calcium in CCTA is based on its small size (<3 mm) and high CT attenuation (>130HU), (Figs. 1, panels b and e and 2, panel a) [29, 49, 67].

Van Velzel el at. have studied 112 patients (53 with ACS, 59 with SAP) further stratified potty calcium into small (<1 mm), intermediate (1-3 mm) and large spotty calcium (>3 mm) [68]. According to their observations small spotty calcium showed the strongest association with vulnerable plaque features as defined by VH-IVUS [68]. Numerous clinical investigations have demonstrated that spotty calcium was more frequent in plaques associated with ACS as compared to plaques in patients with SAP [27, 49, 50, 69]. However, the frequency of spotty calcium varies widely across these studies, demonstrating uncertainty in the relationship between rupture prone lesions and spotty calcium. With further improvements in spatial resolution of the CT scanners, the detection of microcalcification might become feasible, which have the potential to improve the detection of high-risk plaques with CCTA.

Napkin-ring Sign

A recent histopathologic investiagtion by Narula et al. has demonstrated that among plaque features that are potentially accessible by non-invasive imaging the size of necrotic core and the local inflammation (macrophage infiltration) are the two best discriminators between ruptured plaque/TCFA and stable plaques [70••]. A ruptured plaque and TCFA could be separated from fibroatheromas by the presence of a large necrotic core (>3.5 mm^2) [70••]. Thus it is safe to assume that state-of-the-art CT scanners might be able to depict large necrotic cores. The necrotic core contains abundant lipid-rich material, therefore a plaque cross-section with a sizable area of low CT numbers adjacent to the lumen might be indicative of a plaque with a large necrotic core. An intraplaque attenuation pattern with low CT numbers in the central part of the plaque cross-section surrounded by a ring-like higher attenuation plaque area was observed in culprit plaques of patients with ACS [27, 41, 42, 59, 71, 72]. The term napkin-ring sign (NRS) was coined specifically for this plaque attenuation pattern [73]. The NRS is a qualitative plaque feature. No CT attenuation measurement is needed to identify a NRS lesion. As noted previously HU measurements are highly influenced by several factors, among other intraluminal iodinated contrast agent concentration, tube voltage and reconstruction setting used. However, the typical NRS intraplaque CT attenuation pattern can be easily identified in a non-calcified plaque cross-section by the presence of two features: (1) a central area of low CT attenuation that is apparently in contact with the lumen; (2) this same area is surrounded by a ring-like higher attenuation plaque tissue (Fig. 3) [73–75]. An *ex vivo* investiagtion of human hearts demonstrated that the NRS is both visible in non-contast enhanced (native) and in contrast-enhanced images, which suggests that this plaque pattern is caused by the difference in CT attenuation between the large, lipid laden necrotic core and the surrounding ring-like fibrous tissue [73–75]. However, it is important to note that *in vivo* the NRS appearance might be influenced by additional factors such as vasa vasorum [59]. A subsequent *ex vivo* study demonstrated that the NRS plaque pattern had an excellent specificity (98.9 %) to identify advanced atherosclerotic coronary plaques and a poor sensitivity (24.4 %) [74]. The excellent specificity is useful to rule-in high-risk lesions, in order to initiate therapeutic interventions (e.g. intensified statin therapy).

In line with the *ex vivo* observations the NRS pattern showed a 96-100 % specificity to identify TCFA or culprit lesions in a clinical investigation of patients with ACS [27, 28]. A recently published longitudinal study by Otsuka et al. has enrolled 895 patients who underwent CCTA examination. During the mean follow-up period of 2.3 years, the presence of NRS pattern was an independent predictor of acute coronary events (hazard ratio of 5.6, $p<0.0001$) [76••].

Functional Plaque Characteristics

CCTA allows ruling out coronary artery disease with a high negative predictive value [77]. However, the number of false positive findings is relatively high, as the majority of significant stenoses detected by CCTA do not cause ischemia [78]. Large randomized controlled trials have demonstrated that fractional flow reserve (FFR) is able to determine the lesion-specific ischemia, and it is a valuable adjunct to anatomic assessment of coronary atherosclerosis using invasive coronary angiography [79–82].

Adding functional data to anatomical information may help to increase the specificity of CCTA to identify lesions with hemodynamic significance. Computational fluid dynamics (CFD) is a novel method that permits the simulation of coronary blood flow and luminal pressure alterations based on CCTA derived 3-dimensional coronary geometry, which allows the calculation of lesion specific FFR values [83]. Importantly, CFD calculations can be applied on a typically acquired CCTA scan, without any modification of CCTA protocols, additional image acquisition, or administration of medications [83]. In the Diagnosis of Ischemia-Causing Stenoses Obtained Via Noninvasive Fractional Flow Reserve (DISCOVER-FLOW) trial the CT derived FFR calculation (FFR-CT) was compared with invasive FFR, and yielded a per-vessel accuracy, sensitivity, specificity, positive predictive

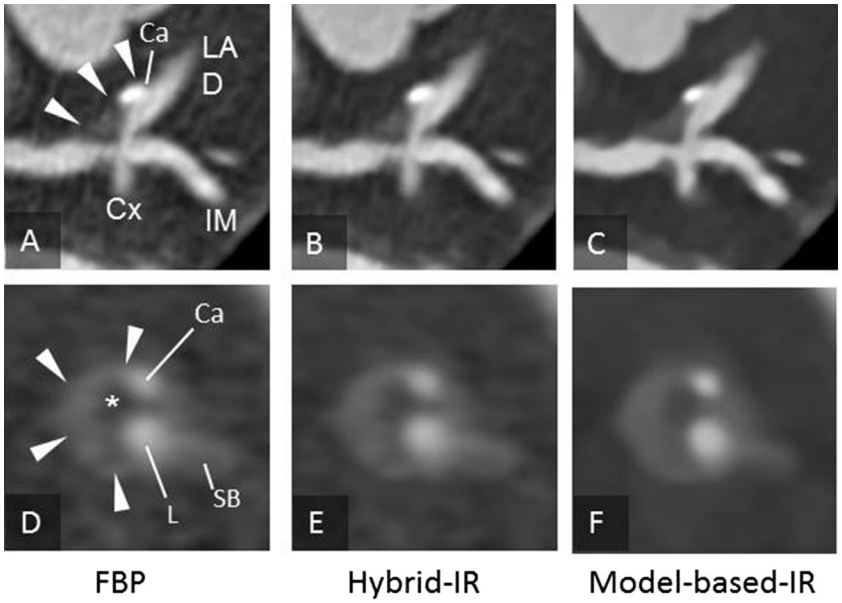

Fig. 3 Double oblique reformations of CCTA images represent longitudinal sections of a partially calcified plaque (*arrowheads*) in LM trifurcation (upper image panels) and cross-sections of the same plaque (lower panels). In the cross-sectional view the plaque shows a NRS attenuation pattern. The low attenuation central region (*star*) of the plaque is surrounded by a ring like area of higher attenuation plaque components (*arrowheads*, panel **d**). Panels **a** and **d**: filtered back projection. Panels B and E: hybrid iterative reconstruction (hybrid-IR). Panels **c** and **f**: model based iterative reconstruction (model-based-IR). *CCTA* coronary computed tomography angiography, *LAD* left anterior descending coronary artery, *LM* left main stem, *IM* ramus intermedius, *Cx* left circumflex coronary artery, *Ca* calcium, *SB* side branch, *L* lumen

value (PPV), and negative predictive value (NPV) for lesions causing ischemia of 84.3 %, 87.9 %, 82.2 %, 73.9 %, and 92.2 %, respectively [83]. In addition, FFR-CT had better diagnostic performance than CCTA alone in the identification of significant coronary lesions [83]. More recently, the Determination of Fractional Flow Reserve by Anatomic Computed Tomographic Angiography (DeFACTO) trial has enrolled 252 patients and demonstrated that FFR-CT was superior to CCTA in identifying ischemic lesions (accuracy [73 % vs. 64 %], sensitivity [90 % vs. 84 %], specificity [54 % vs. 42 %], PPV [67 % vs. 61 %], and NPV [84 % vs. 72 %]).

Recently, a histopathologic study has demonstrated that around 50 % of TCFAs produce an intermediate (50 % to 75 %) luminal area stenosis [70••]. Notably, about half of the intermediate lesions cause significant ischemia and the other half not, which demonstrates that the relationship between stenosis and ischemia is unreliable [84]. It has been proposed that in a setting of an intermediate lesion with abnormal FFR, the flow perturbations and the altered endothelial shear stress might be responsible for the development of rupture prone lesion [85, 86]. In fact, this is in line with the vast body of evidence regarding the poor prognosis of patients with ischemic lesions [87, 88]. Therefore, we can hypothesize it is safe to assume that FFR as derived from CCTA (FFR-CT) will not only help to identify luminal narrowing with significant ischemia, but it will improve the accuracy of CT to detect lesions with an increased risk to cause acute coronary event.

Plaques tend to develop at specific locations in the coronary arteries, even though promoting cardiovascular risk factors for coronary plaque formation affect the vascular bed systemically. The inner curvature of coronaries, the outer waist of bifurcations and the side-branches are predilection sites for atherogenesis. At these locations the endothelial shear stress (ESS) is low and the flow is disturbed or turbulent [89–93]. Where ESS is low, the endothelial cell gene expression shifts towards a pro-atherogenic pattern, which subsequently leads to the development of high-risk lesions [92, 94]. In the recently published Prediction of Progression of Coronary Artery Disease and Clinical Outcome Using Vascular Profiling of Shear Stress and Wall Morphology (PREDICTION), a total of 506 patients underwent three vessel IVUS examination and were followed-up for 1 year [95]. Stone et al. demonstrated that low ESS and large plaque burden independently predict plaque progression [96]. It has been shown that the application of CFD on CCTA images enables the calculation of ESS and the generation of 3D ESS-CT maps [97–100]. In a recent clinical investigation CCTA demonstrated sufficient accuracy to study the ESS distribution in the main vessels and in the bifurcation regions as compared to IVUS vascular profiling [101]. The assessment of ESS-CT might be an important addition to morphological CCTA plaque features to improve risk stratification. The comprehensive assessment of ESS-CT and FFR-CT might provide a novel functional dimension in plaque vulnerability assessment in CCTA. This combined anatomic-physiological evaluation of coronary plaques with CCTA may allow to develop novel stratified therapeutic approaches to treat vulnerable plaques and ultimately to improve event-free survival.

Novel Technical Developments in CT Plaque Assessment

Improvements in CT technology, the use of hybrid techniques and novel image reconstruction algorithms may improve non-invasive coronary plaque characterization through providing images with improved spatial and contrast resolution and adding metabolic information to morphological plaque assessment. Dual-energy CT (DECT) is a promising technique for advanced tissue characterization, first applied in the 1970s, and is based on the physical principle that tissue attenuation values change at different energy levels of X-ray [102, 103]. The recording of spectrally different attenuation datasets enable the visualization and quantification of blood supply in the myocardium and may also benefit the discrimination of atherosclerotic plaque components [104]. Vendors have developed different approaches for spectral imaging. The most clinical data regarding the cardiac applications of DECT is available with simultaneous application of two X-ray tubes at different peak voltage [105, 106]. Ruzsics et al. investigated 35 patients and were able to detect myocardial ischemia with a high degree of accuracy [105]. Another approach is the use of rapid kV switching between two different peak voltage levels by one X-ray tube during the scan [107]. The latest, photon-counting technique (also known as spectral CT) applies panels of energy sensitive detectors to capture X-ray photons both at low and high energy levels, whereas only one X-ray tube is operated at a distinct tube voltage [104]. Recently, the feasibility of atherosclerotic plaque characterization was demonstrated with phase-contrast CT in an animal study [108]. Phase contrast CT uses phase shift of x-rays passing through matter to generate tissue contras [109, 110]. This experimental imaging techniques has a great potential to improve contrast resolution as its sensitivity to light elements is almost 1000 times greater than that of the conventional absorption-contrast X-ray method [105].

Novel nanotechnology contrast agents have a great potential to identify inflammatory cell infiltration of the fibrous cap, which is a strong marker of plaque vulnerability [53]. Hyafil et al. demonstrated that the CCTA inflammatory cell detection is feasible in atherosclerotic plaques with iodinated nanoparticle contrast agent N1117 [111]. Gold-labeled high density lipoprotein (Au-HDL) nanoparticles designed to target activated macrophages imaged by spectral CT showed promising results in atherosclerotic mice model [112].

Macrophages have a high metabolic activity and they depend on exogenous glucose for their metabolism, therefore using radiolabeled glucose analog, fluorine-18-fluorodeoxyglucose (^{18}F-FDG) to non-invasively detect vulnerable, inflamed plaques might be feasible with hybrid positron emission tomography (PET) and CT imaging (PET-CT). Rogers et al. observed an increased ^{18}F-FDG accumulation at the culprit lesion site of patients with recent ACS as compared to lesions in patients with

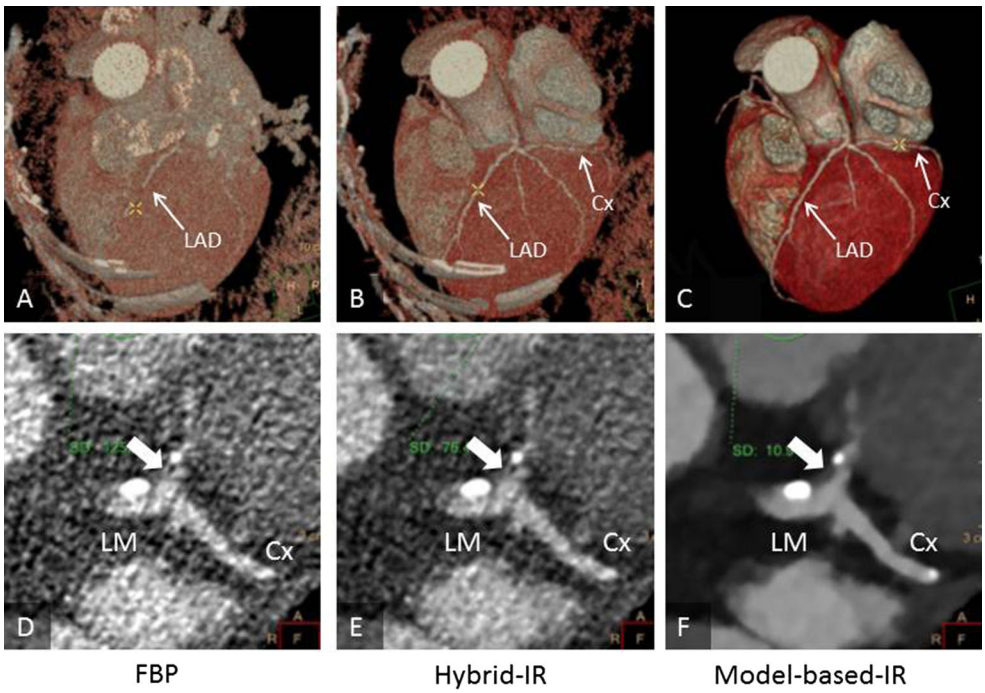

Fig. 4 CCTA images of an obese patient (BMI: 41 kg/m^2). The figure shows volume rendered reformations of CCTA images (upper panels) and axial images at the height of the LM bifurcation (lower panels). The *white arrow* indicates non-calcified plaque component of the partially calcified plaque in the LM bifurcation. The plaque components are clearly visible with model based iterative reconstruction (panel **f**), whereas the differentiation between different plaque components is limited with FBP and Hybrid-IR due to the low CNR (panels **d** and **e**). *CCTA* coronary computed tomography angiography, *LAD* left anterior descending coronary artery, *LM* left main stem, *Cx* left circumflex coronary artery, *FBP* filtered back projection recosntruction, *IR* iterative reconstruction, *CNR* contrast-to-noise ratio

SAP [113]. In a recently published clinical trial Joshi et al. demonstrated that ^{18}F-NaF PET-CT imaging allows the detection of metabolically active plaques by identifying areas of ongoing calcification activity [114••]. Metabolic imaging with hybrid techniques or nanoparticle contrast agents might shed light on the molecular aspects of coronary atherosclerosis and vulnerable plaque.

In the 1980s filtered back projection (FBP) became the standard of image reconstruction technique, because it is fast, reliable and can be performed even with limited computer processing capabilities. However, the concerns regarding ionizing radiation and the available high computational power pushed vendors to develop novel image reconstruction algorithms. While in the reconstruction process with FBP assumptions are made regarding system geometry and image reliability weakens with increased noise, iterative reconstruction (IR) techniques were developed by modelling system geometry, physics and noise statistics to achieve improved image quality [115–117]. Through repetitive reconstruction cycles (iterations), the image reconstructed from the actually measured data projection is compared to a forward projected image, simulating an ideal data acquisition. The differences among the true and simulated reconstruction help to update the original image with optimal noise reduction, while image contrast is preserved [118]. The hybrid iterative reconstruction uses data reconstructed with FBP, thus the iterations are performed in the image space, which is less time consuming [119, 120]. The reduced image noise allows scanning with reduced tube current and tube voltage, which results in significant dose reduction (up to 44-63 % reduction in effective radiation dose) [121–123]. In addition, it has recently been demonstrated that IR significantly improves objective image quality [124, 125]. Furthermore, Renker et al. investigated 55 patients with Agatston scores >400, who underwent CCTA and invasive coronary angiography. They found that IR has reduced blooming artifacts in heavily calcified lesions and improved diagnostic performance of CCTA to identify obstructive coronary plaques [126]. More advanced, model-based iterative reconstruction techniques have been introduced recently [118, 127]. Model based IR is a true 3D, raw-data based image reconstruction technique, which improves image resolution through increased point spread function [118]. Moreover, it has shown superior image quality and increased contrast-to-noise ratio as compared to FBP and hybrid-IR (Fig. 3) [118]. Model based image reconstruction improved the performance of automated coronary plaque assessment tools [127], and it has a potential to improve plaque visualization and characterization in the clinical setting (Fig. 4).

Conclusion

CCTA is a unique non-invasive imaging technique that allows the visualization of all main epicardial coronary arteries. It can assess individual coronary plaques as well as the global coronary plaque burden. The quantitative and qualitative high-risk plaque features in CCTA are associated with acute coronary events. Positive remodelling, low CT attenuation, napkin-ring sign, spotty calcification are morphological features, whereas ESS-CT and FFR-CT provide functional data regarding individual atherosclerotic lesions. Nanoparticle contrast agents and hybrid imaging techniques have a great potential to add valuable information regarding inflammation and metabolic activity at the site of atherosclerotic plaques. Large prospective trials are warranted to confirm the observations of smaller and to assess the effectiveness of image guided therapeutic approaches based on CCTA.

Acknowledgments The authors thank Rolf Raaijmakers for the images processed with model based iterative reconstruction. This work was supported by the European Union and the State of Hungary, co-financed by the European Social Fund in the framework of TÁMOP 4.2.4. A/1-11-1-2012-0001 'National Excellence Program'.

Compliance with Ethics Guidelines

Conflict of Interest Andrea Bartykowszki, Csilla Celeng, Mihály Károlyi, and Pál Maurovich-Horvat declare that they have no conflict of interest.

Human and Animal Rights and Informed Consent This article does not contain any studies with human or animal subjects performed by any of the authors.

References

Papers of particular interest, published recently, have been highlighted as:
•• Of major importance

1. Go AS et al. Heart disease and stroke statistics–2014 update: a report from the American Heart Association. Circulation. 2014;129(3):e28–e292.
2. Falk E. Pathogenesis of atherosclerosis. J Am Coll Cardiol. 2006;47(8 Suppl):C7–C12.
3. Hansson GK. Inflammation, atherosclerosis, and coronary artery disease. N Engl J Med. 2005;352(16):1685–95.
4. Libby P. Atherosclerosis: the new view. Sci Am. 2002;286(5):46–55.
5. Burke AP et al. Coronary risk factors and plaque morphology in men with coronary disease who died suddenly. N Engl J Med. 1997;336(18):1276–82.
6. Falk E et al. Update on acute coronary syndromes: the pathologists' view. Eur Heart J. 2013;34(10):719–28.
7. Virmani R et al. Lessons from sudden coronary death: a comprehensive morphological classification scheme for atherosclerotic lesions. Arterioscler Thromb Vasc Biol. 2000;20(5):1262–75.
8. Narula J, Achenbach S. Napkin-ring necrotic cores: defining circumferential extent of necrotic cores in unstable plaques. J Am Coll Cardiol Img. 2009;2(12):1436–8.

9. Alkadhi H et al. Low-dose, 128-slice, dual-source CT coronary angiography: accuracy and radiation dose of the high-pitch and the step-and-shoot mode. Heart. 2010;96(12):933–8.
10. Sun Z, Ng KH. Diagnostic value of coronary CT angiography with prospective ECG-gating in the diagnosis of coronary artery disease: a systematic review and meta-analysis. Int J Cardiovasc Imaging. 2012;28(8):2109–19.
11. Miller JM et al. Diagnostic performance of coronary angiography by 64-row CT. N Engl J Med. 2008;359(22):2324–36.
12. Muller JE, Tofler GH, Stone PH. Circadian variation and triggers of onset of acute cardiovascular disease. Circulation. 1989;79(4): 733–43.
13. Virmani R et al. Pathology of the vulnerable plaque. J Am Coll Cardiol. 2006;47(8 Suppl):C13–8.
14. van der Giessen AG et al. Small coronary calcifications are not detectable by 64-slice contrast enhanced computed tomography. Int J Cardiovasc Imaging. 2011;27(1):143–52.
15. Stone GW et al. A prospective natural-history study of coronary atherosclerosis. N Engl J Med. 2011;364(3):226–35.
16. Maurovich-Horvat P et al. Methods of plaque quantification and characterization by cardiac computed tomography. J Cardiovasc Comput Tomogr. 2009;3 Suppl 2:S91–8.
17. Schepis T et al. Comparison of dual source computed tomography versus intravascular ultrasound for evaluation of coronary arteries at least one year after cardiac transplantation. Am J Cardiol. 2009;104(10):1351–6.
18. Brodoefel H et al. Coronary plaque quantification by voxel analysis: dual-source MDCT angiography versus intravascular sonography. AJR Am J Roentgenol. 2009;192(3):W84–9.
19. Petranovic M et al. Assessment of nonstenotic coronary lesions by 64-slice multidetector computed tomography in comparison to intravascular ultrasound: evaluation of nonculprit coronary lesions. J Cardiovasc Comput Tomogr. 2009;3(1):24–31.
20. Sun J et al. Identification and quantification of coronary atherosclerotic plaques: a comparison of 64-MDCT and intravascular ultrasound. AJR Am J Roentgenol. 2008;190(3):748–54.
21.•• Voros S et al. Coronary atherosclerosis imaging by coronary CT angiography: current status, correlation with intravascular interrogation and meta-analysis. J Am Coll Cardiol Img. 2011;4(5):537–48. *A comprehensive review on the CCTA based quantitative and qualitative plaque characterization*.
22. Leber AW et al. Accuracy of 64-slice computed tomography to classify and quantify plaque volumes in the proximal coronary system: a comparative study using intravascular ultrasound. J Am Coll Cardiol. 2006;47(3):672–7.
23. Hur J et al. Quantification and characterization of obstructive coronary plaques using 64-slice computed tomography: a comparison with intravascular ultrasound. J Comput Assist Tomogr. 2009;33(2):186–92.
24.•• Boogers MJ et al. Automated quantification of coronary plaque with computed tomography: comparison with intravascular ultrasound using a dedicated registration algorithm for fusion-based quantification. Eur Heart J. 2012;33(8):1007–16. *This study demonstrated the feasibility of semiautomated quantification of coronary plaque burden with CCTA. Quantitative computed tomography and IVUS showed good correlation*.
25. Voros S et al. Prospective validation of standardized, 3-dimensional, quantitative coronary computed tomographic plaque measurements using radiofrequency backscatter intravascular ultrasound as reference standard in intermediate coronary arterial lesions: results from the ATLANTA (assessment of tissue characteristics, lesion morphology, and hemodynamics by angiography with fractional flow reserve, intravascular ultrasound and virtual histology, and noninvasive computed tomography in atherosclerotic plaques) I study. J Am Coll Cardiol Intv. 2011;4(2):198–208.
26. Oberoi S et al. Reproducibility of non-calcified coronary artery plaque burden quantification from coronary CT angiography across different image analysis platforms. AJR Am J Roentgenol. 2014;202(1):W43–9.
27. Pflederer T et al. Characterization of culprit lesions in acute coronary syndromes using coronary dual-source CT angiography. Atherosclerosis. 2010;211(2):437–44.
28. Madder RD et al. Features of disrupted plaques by coronary computed tomographic angiography: correlates with invasively proven complex lesions. Circ Cardiovasc Imaging. 2011;4(2): 105–13.
29. Motoyama S et al. Computed tomographic angiography characteristics of atherosclerotic plaques subsequently resulting in acute coronary syndrome. J Am Coll Cardiol. 2009;54(1):49–57.
30.•• Kristensen TS et al. Prognostic implications of nonobstructive coronary plaques in patients with non-ST-segment elevation myocardial infarction: a multidetector computed tomography study. J Am Coll Cardiol. 2011;58(5):502–9. *This prospective study demonstrated that the total amount of non-calcified plaque independently associated with an increased risk of recurrent coronary events after NSTEMI*.
31. Versteylen MO et al. Additive value of semiautomated quantification of coronary artery disease using cardiac computed tomographic angiography to predict future acute coronary syndrome. J Am Coll Cardiol. 2013;61(22):2296–305.
32. Narula J et al. Arithmetic of vulnerable plaques for noninvasive imaging. Nat Clin Pract Cardiovasc Med. 2008;5 Suppl 2:S2–S10.
33. Kopp AF et al. Non-invasive characterisation of coronary lesion morphology and composition by multislice CT: first results in comparison with intracoronary ultrasound. Eur Radiol. 2001;11(9):1607–11.
34. Schroeder S et al. Noninvasive detection and evaluation of atherosclerotic coronary plaques with multislice computed tomography. J Am Coll Cardiol. 2001;37(5):1430–5.
35. Becker CR et al. Ex vivo coronary atherosclerotic plaque characterization with multi-detector-row CT. Eur Radiol. 2003;13(9): 2094–8.
36. Leber AW et al. Accuracy of multidetector spiral computed tomography in identifying and differentiating the composition of coronary atherosclerotic plaques: a comparative study with intracoronary ultrasound. J Am Coll Cardiol. 2004;43(7):1241–7.
37. Pohle K et al. Characterization of non-calcified coronary atherosclerotic plaque by multi-detector row CT: comparison to IVUS. Atherosclerosis. 2007;190(1):174–80.
38. Ferencik M et al. Arterial wall imaging: evaluation with 16-section multidetector CT in blood vessel phantoms and ex vivo coronary arteries. Radiology. 2006;240(3):708–16.
39. Gauss S et al. Assessment of coronary artery remodelling by dual-source CT: a head-to-head comparison with intravascular ultrasound. Heart. 2011;97(12):991–7.
40. Schlett CL et al. Histogram analysis of lipid-core plaques in coronary computed tomographic angiography: ex vivo validation against histology. Investig Radiol. 2013;48(9):646–53.
41. Kashiwagi M et al. Feasibility of noninvasive assessment of thin-cap fibroatheroma by multidetector computed tomography. J Am Coll Cardiol Img. 2009;2(12):1412–9.
42. Ito T et al. Comparison of in vivo assessment of vulnerable plaque by 64-slice multislice computed tomography versus optical coherence tomography. Am J Cardiol. 2011;107(9):1270–7.
43. Ito H, et al. Characteristics of plaque progression detected by serial coronary computed tomography angiography. Heart and vessels, 2013. doi:10.1007/s00380-013-0420-4.
44. Viles-Gonzalez JF et al. In vivo 16-slice, multidetector-row computed tomography for the assessment of experimental atherosclerosis: comparison with magnetic resonance imaging and histopathology. Circulation. 2004;110(11):1467–72.

45. Achenbach S et al. Influence of slice thickness and reconstruction kernel on the computed tomographic attenuation of coronary atherosclerotic plaque. J Cardiovasc Comput Tomogr. 2010;4(2):110–5.
46. Cademartiri F et al. Influence of intracoronary attenuation on coronary plaque measurements using multislice computed tomography: observations in an ex vivo model of coronary computed tomography angiography. Eur Radiol. 2005;15(7):1426–31.
47. Suzuki S et al. Accuracy of attenuation measurement of vascular wall in vitro on computed tomography angiography: effect of wall thickness, density of contrast medium, and measurement point. Investig Radiol. 2006;41(6):510–5.
48. Achenbach S et al. CV imaging: what was new in 2012? JACC Cardiovasc Imaging. 2013;6(6):714–34.
49. Motoyama S et al. Multislice computed tomographic characteristics of coronary lesions in acute coronary syndromes. J Am Coll Cardiol. 2007;50(4):319–26.
50. Kim SY et al. The culprit lesion score on multi-detector computed tomography can detect vulnerable coronary artery plaque. Int J Cardiovasc Imaging. 2010;26 Suppl 2:245–52.
51. Kitagawa T et al. Characterization of non-calcified coronary plaques and identification of culprit lesions in patients with acute coronary syndrome by 64-slice computed tomography. JACC Cardiovasc Imaging. 2009;2(2):153–60.
52. Glagov S et al. Compensatory enlargement of human atherosclerotic coronary arteries. N Engl J Med. 1987;316(22):1371–5.
53. Narula J, Strauss HW. The popcorn plaques. Nat Med. 2007;13(5):532–4.
54.•• Libby P. Mechanisms of acute coronary syndromes and their implications for therapy. N Engl J Med. 2013;368(21):2004–13. *A comprehensive overview of the pathophysiology and latest therapeutic implications of acut coronary syndrome*.
55. Achenbach S et al. Assessment of coronary remodelling in stenotic and nonstenotic coronary atherosclerotic lesions by multidetector spiral computed tomography. J Am Coll Cardiol. 2004;43(5):842–7.
56. Mintz GS et al. American College of Cardiology Clinical Expert Consensus Document on Standards for Acquisition, Measurement and Reporting of Intravascular Ultrasound Studies (IVUS). A report of the American College of Cardiology Task Force on Clinical Expert Consensus Documents. J Am Coll Cardiol. 2001;37(5):1478–92.
57. Kroner ES et al. Positive remodelling on coronary computed tomography as a marker for plaque vulnerability on virtual histology intravascular ultrasound. Am J Cardiol. 2011;107(12):1725–9.
58. Otsuka F, Finn AV, Virmani R. Do vulnerable and ruptured plaques hide in heavily calcified arteries? Atherosclerosis. 2013;229(1):34–7.
59. Nakazawa G et al. Efficacy of culprit plaque assessment by 64-slice multidetector computed tomography to predict transient no-reflow phenomenon during percutaneous coronary intervention. Am Heart J. 2008;155(6):1150–7.
60. Taylor AJ et al. Coronary calcium independently predicts incident premature coronary heart disease over measured cardiovascular risk factors: mean three-year outcomes in the Prospective Army Coronary Calcium (PACC) project. J Am Coll Cardiol. 2005;46(5):807–14.
61. Greenland P et al. Coronary artery calcium score combined with Framingham score for risk prediction in asymptomatic individuals. JAMA. 2004;291(2):210–5.
62. Huang H et al. The impact of calcification on the biomechanical stability of atherosclerotic plaques. Circulation. 2001;103(8):1051–6.
63. Mauriello A et al. Coronary calcification identifies the vulnerable patient rather than the vulnerable Plaque. Atherosclerosis. 2013;229(1):124–9.
64. Maldonado N et al. A mechanistic analysis of the role of microcalcifications in atherosclerotic plaque stability: potential implications for plaque rupture. Am J Physiol Heart Circ Physiol. 2012;303(5):H619–28.
65. Kataoka Y et al. Spotty calcification as a marker of accelerated progression of coronary atherosclerosis: insights from serial intravascular ultrasound. J Am Coll Cardiol. 2012;59(18):1592–7.
66. Ehara S et al. Spotty calcification typifies the culprit plaque in patients with acute myocardial infarction: an intravascular ultrasound study. Circulation. 2004;110(22):3424–9.
67. Ferencik M et al. A computed tomography-based coronary lesion score to predict acute coronary syndrome among patients with acute chest pain and significant coronary stenosis on coronary computed tomographic angiogram. Am J Cardiol. 2012;110(2):183–9.
68. van Velzen JE et al. Comprehensive assessment of spotty calcifications on computed tomography angiography: comparison to plaque characteristics on intravascular ultrasound with radiofrequency backscatter analysis. J Nucl Cardiol Off Publ Am Soc Nucl Cardiol. 2011;18(5):893–903.
69. Ozaki Y et al. Coronary CT angiographic characteristics of culprit lesions in acute coronary syndromes not related to plaque rupture as defined by optical coherence tomography and angioscopy. Eur Heart J. 2011;32(22):2814–23.
70.•• Narula J et al. Histopathologic characteristics of atherosclerotic coronary disease and implications of the findings for the invasive and noninvasive detection of vulnerable plaques. J Am Coll Cardiol. 2013;61(10):1041–51. *This postmortem study analized 295 coronary atherosclerotic plaques to define histomorphologic characteristics of vulnerable plaques and suggests that plaques that rupture cause substantial luminal narrowing before the acute event*.
71. Kodama T et al. Computed tomographic angiography-verified plaque characteristics and slow-flow phenomenon during percutaneous coronary intervention. JACC Cardiovasc Interv. 2012;5(6):636–43.
72. Tanaka A et al. Non-invasive assessment of plaque rupture by 64-slice multidetector computed tomography–comparison with intravascular ultrasound. Circ J. 2008;72(8):1276–81.
73. Maurovich-Horvat P et al. The napkin-ring sign: CT signature of high-risk coronary plaques? JACC. Cardiovascular Imaging. 2010;3(4):440–4.
74. Maurovich-Horvat P et al. The napkin-ring sign indicates advanced atherosclerotic lesions in coronary CT angiography. J Am Coll Cardiol Img. 2012;5(12):1243–52.
75. Seifarth H et al. Histopathological correlates of the napkin-ring sign plaque in coronary CT angiography. Atherosclerosis. 2012;224(1):90–6.
76.•• Otsuka K et al. Napkin-ring sign on coronary CT angiography for the prediction of acute coronary syndrome. J Am Coll Cardiol Img. 2013;6(4):448–57. *The first prospective study which demonstrated that the napkin-ring sign on the CCTA is strongly associated with future ACS events*.
77. Achenbach S. Computed tomography coronary angiography. J Am Coll Cardiol. 2006;48(10):1919–28.
78. Meijboom WB et al. Comprehensive assessment of coronary artery stenoses: computed tomography coronary angiography versus conventional coronary angiography and correlation with fractional flow reserve in patients with stable angina. J Am Coll Cardiol. 2008;52(8):636–43.
79. De Bruyne B et al. Coronary flow reserve calculated from pressure measurements in humans. Validation with positron emission tomography. Circulation. 1994;89(3):1013–22.
80. Berger A et al. Long-term clinical outcome after fractional flow reserve-guided percutaneous coronary intervention in patients with multivessel disease. J Am Coll Cardiol. 2005;46(3):438–42.

81. Tonino PA et al. Fractional flow reserve versus angiography for guiding percutaneous coronary intervention. N Engl J Med. 2009;360(3):213–24.
82. Pijls NH et al. Experimental basis of determining maximum coronary, myocardial, and collateral blood flow by pressure measurements for assessing functional stenosis severity before and after percutaneous transluminal coronary angioplasty. Circulation. 1993;87(4):1354–67.
83. Koo BK et al. Diagnosis of ischemia-causing coronary stenoses by noninvasive fractional flow reserve computed from coronary computed tomographic angiograms. Results from the prospective multicenter DISCOVER-FLOW (Diagnosis of Ischemia-Causing Stenoses Obtained Via Noninvasive Fractional Flow Reserve) study. J Am Coll Cardiol. 2011;58(19):1989–97.
84. Bech GJ et al. Fractional flow reserve to determine the appropriateness of angioplasty in moderate coronary stenosis: a randomized trial. Circulation. 2001;103(24):2928–34.
85. Fearon WF. Is a myocardial infarction more likely to result from a mild coronary lesion or an ischemia-producing one? Circ Cardiovasc Interv. 2011;4(6):539–41.
86. Gijsen FJ et al. Strain distribution over plaques in human coronary arteries relates to shear stress. Am J Physiol Heart Circ Physiol. 2008;295(4):H1608–14.
87. Hachamovitch R et al. Value of stress myocardial perfusion single photon emission computed tomography in patients with normal resting electrocardiograms: an evaluation of incremental prognostic value and cost-effectiveness. Circulation. 2002;105(7):823–9.
88. Shaw LJ et al. Optimal medical therapy with or without percutaneous coronary intervention to reduce ischemic burden: results from the Clinical Outcomes Utilizing Revascularization and Aggressive Drug Evaluation (COURAGE) trial nuclear substudy. Circulation. 2008;117(10):1283–91.
89. Caro CG, Fitz-Gerald JM, Schroter RC. Arterial wall shear and distribution of early atheroma in man. Nature. 1969;223(5211):1159–60.
90. Friedman MH et al. Correlation between wall shear and intimal thickness at a coronary artery branch. Atherosclerosis. 1987;68(1–2):27–33.
91. Koskinas KC et al. Natural history of experimental coronary atherosclerosis and vascular remodelling in relation to endothelial shear stress: a serial, in vivo intravascular ultrasound study. Circulation. 2010;121(19):2092–101.
92. Malek AM, Alper SL, Izumo S. Hemodynamic shear stress and its role in atherosclerosis. JAMA. 1999;282(21):2035–42.
93. Wentzel JJ et al. Endothelial shear stress in the evolution of coronary atherosclerotic plaque and vascular remodelling: current understanding and remaining questions. Cardiovasc Res. 2012;96(2):234–43.
94. Chatzizisis YS et al. Role of endothelial shear stress in the natural history of coronary atherosclerosis and vascular remodelling: molecular, cellular, and vascular behavior. J Am Coll Cardiol. 2007;49(25):2379–93.
95. Dey D et al. Automated three-dimensional quantification of non-calcified coronary plaque from coronary CT angiography: comparison with intravascular US. Radiology. 2010;257(2):516–22.
96. Stone PH et al. Prediction of progression of coronary artery disease and clinical outcomes using vascular profiling of endothelial shear stress and arterial plaque characteristics: the PREDICTION Study. Circulation. 2012;126(2):172–81.
97. Frauenfelder T et al. In-vivo flow simulation in coronary arteries based on computed tomography datasets: feasibility and initial results. Eur Radiol. 2007;17(5):1291–300.
98. Jin S et al. Flow patterns and wall shear stress distributions at atherosclerotic-prone sites in a human left coronary artery–an exploration using combined methods of CT and computational fluid dynamics. Conf Proc IEEE Eng Med Biol Soc. 2004;5:3789–91.
99. Borkin MA et al. Evaluation of artery visualizations for heart disease diagnosis. IEEE Trans Vis Comput Graph. 2011;17(12):2479–88.
100. Ramkumar PG et al. New advances in cardiac computed tomography. Curr Opin Cardiol. 2009;24(6):596–603.
101. Gijsen FJ et al. 3D reconstruction techniques of human coronary bifurcations for shear stress computations. J Biomech. 2014;47(1):39–43.
102. McCullough EC. Photon attenuation in computed tomography. Med Phys. 1975;2(6):307–20.
103. Alvarez RE, Macovski A. Energy-selective reconstructions in X-ray computerized tomography. Phys Med Biol. 1976;21(5):733–44.
104. Halliburton SS. Recent technologic advances in multi-detector row cardiac CT. Cardiol Clin. 2009;27(4):655–64.
105. Ruzsics B et al. Dual-energy CT of the heart for diagnosing coronary artery stenosis and myocardial ischemia-initial experience. Eur Radiol. 2008;18(11):2414–24.
106. Schwarz F et al. Dual-energy CT of the heart–principles and protocols. Eur J Radiol. 2008;68(3):423–33.
107. So A et al. Prospectively ECG-triggered rapid kV-switching dual-energy CT for quantitative imaging of myocardial perfusion. JACC Cardiovasc Imaging. 2012;5(8):829–36.
108. Shinohara M et al. Atherosclerotic plaque imaging using phase-contrast X-ray computed tomography. Am J Physiol Heart Circ Physiol. 2008;294(2):H1094–100.
109. Momose A, Fukuda J. Phase-contrast radiographs of nonstained rat cerebellar specimen. Med Phys. 1995;22(44):6355–67.
110. Fitzgerald R. Phase-sensitive x-ray imaging. Phys Today. 2000;53(7):23–6.
111. Hyafil F et al. Quantification of inflammation within rabbit atherosclerotic plaques using the macrophage-specific CT contrast agent N1177: a comparison with 18F-FDG PET/CT and histology. J Nucl Med. 2009;50(6):959–65.
112. Cormode DP et al. Atherosclerotic plaque composition: analysis with multicolor CT and targeted gold nanoparticles. Radiology. 2010;256(3):774–82.
113. Rogers IS et al. Feasibility of FDG imaging of the coronary arteries: comparison between acute coronary syndrome and stable angina. JACC Cardiovasc Imaging. 2010;3(4):388–97.
114.•• Joshi NV et al. 18F-fluoride positron emission tomography for identification of ruptured and high-risk coronary atherosclerotic plaques: a prospective clinical trial. Lancet. 2014;383(9918):705–13. *In this prospective clinical trial the authors have shown that intense 18F-NaF uptake localises to recent plaque rupture in patients with acute myocardial infarction.*
115. Marin D et al. Low-tube-voltage, high-tube-current multidetector abdominal CT: improved image quality and decreased radiation dose with adaptive statistical iterative reconstruction algorithm–initial clinical experience. Radiology. 2010;254(1):145–53.
116. Prakash P et al. Diffuse lung disease: CT of the chest with adaptive statistical iterative reconstruction technique. Radiology. 2010;256(1):261–9.
117. Yu Z et al. Fast model-based X-ray CT reconstruction using spatially nonhomogeneous ICD optimization. IEEE Trans Image Process. 2011;20(1):161–75.
118. Scheffel H et al. Coronary artery plaques: cardiac CT with model-based and adaptive-statistical iterative reconstruction technique. Eur J Radiol. 2012;81(3):e363–9.
119. Yoo RE et al. Image quality of adaptive iterative dose reduction 3D of coronary CT angiography of 640-slice CT: comparison with filtered back-projection. Int J Cardiovasc Imaging. 2013;29(3):669–76.
120. Leipsic J, Heilbron BG, Hague C. Iterative reconstruction for coronary CT angiography: finding its way. Int J Cardiovasc Imaging. 2012;28(3):613–20.

121. Benedek T, Gyongyosi M, Benedek I. Multislice computed tomographic coronary angiography for quantitative assessment of culprit lesions in acute coronary syndromes. Can J Cardiol. 2013;29(3):364–71.
122. Leipsic J et al. Estimated radiation dose reduction using adaptive statistical iterative reconstruction in coronary CT angiography: the ERASIR study. AJR Am J Roentgenol. 2010;195(3):655–60.
123. Min JK et al. Diagnostic accuracy of fractional flow reserve from anatomic CT angiography. JAMA. 2012;308(12):1237–45.
124. Takx RA et al. The effect of iterative reconstruction on quantitative computed tomography assessment of coronary plaque composition. Int J Cardiovasc Imaging. 2014;30(1):155–63.
125. Fuchs TA et al. CT coronary angiography: impact of adapted statistical iterative reconstruction (ASIR) on coronary stenosis and plaque composition analysis. Int J Cardiovasc Imaging. 2013;29(3):719–24.
126. Renker M et al. Evaluation of heavily calcified vessels with coronary CT angiography: comparison of iterative and filtered back projection image reconstruction. Radiology. 2011;260(2):390–9.
127. Puchner SB et al. The effect of iterative image reconstruction algorithms on the feasibility of automated plaque assessment in coronary CT angiography. Int J Cardiovasc Imaging. 2013;29(8):1879–88.